Absorption leads to narrower plasmonic resonances

RYAN L. PECK,[1,2], ALEXANDRE G. BROLO,[2,3], REUVEN GORDON,[2, 4*]

[1]*Department of Physics, University of Victoria, 3800 Finnerty Rd, Victoria, BC, Canada*

[2]*Center for Advanced Materials and Related Technologies (CAMTEC), University of Victoria, 3800 Finnerty Rd, Victoria, BC, Canada*

[3]*Department of Chemistry, University of Victoria, 3800 Finnerty Rd, Victoria, BC, Canada*

[4]*Department of Electrical and Computer Engineering, University of Victoria, 3800 Finnerty Rd, Victoria, BC, Canada*

[*]*rgordon@uvic.ca*

Abstract: While it is generally accepted that adding loss dampens and broadens plasmonic resonances, here we find adding losses can actually narrow the linewidth and increase the resonance peak. We show that the scattering cross section of a metal nanoparticle in a lossy dielectric medium is an order of magnitude larger than the same nanoparticle in a lossless dielectric. The full width at half maximum is a quarter of that of the non-absorbing medium. The peak narrowing and increased scattering has benefits for biomarkers where high scattering efficiency and narrow linewidths (for denser multiplexing) is desired. The enhanced scattering and absorption in the surrounding lossy medium is also beneficial for photovoltaic applications.

1. Introduction

Plasmonic resonances have been studied for over a century and have many applications including SERS (surface enhanced Raman scattering) [1–4], optical tweezers [5–7], biosensing [8–11], subwavelength imaging [12–14], waveguiding and nanocircuits [15–19] and photovoltaics [20–23]. For many of these applications it is desirable to have sharp plasmonic resonance peaks [24–26].

The conventional wisdom is that plasmonic peaks are broadened by the addition of material losses [27, 28]. The width of the plasmonic peak is assumed to be directly related to the decay time from losses [29]

$$\Gamma = \frac{2\hbar}{T_2} \tag{1}$$

where Γ is the linewidth of the plasmonic peak, and T_2 is the total decay time.

Many factors influence absorption of light, such as electron scattering [30, 31], surface scattering [32, 33] and chemical interface scattering [34–36]. Studies show that the scattering cross section of individual particles is narrower than the ensemble, suggesting that loss attributed to effects such as surface scattering (the interaction of the oscillating electrons confined in the metal with the boundary of the metal) may be exaggerated [37]. There has certainly been a wide range of values attributed to surface scattering in the literature [34, 38–40], from negligible to significant.

Adding materials with gain ($\mathrm{Im}(\epsilon_2) < 0$) around noble metal nanoparticles can result in more prominent plasmonic peaks [41, 42]. The extreme case of using gain materials for sharper resonances is the SPASER (surface plasmon amplification by stimulated emission of radiation) [43, 44], which produces a very narrow peak and has been touted for applications in biosensing [45]. Surrounding a metal nanoparticle with an absorbing material, the opposite of a gain material, may be considered to have the opposite effect on the resonance linewidth; i.e., the linewidth should be broadened and the plasmonic peak reduced.

A lot of work on solar cells in the literature looked at incorporating nanoparticles in absorbing materials e.g. ([46–48]). There they focussed on absorption and the aim was to get a broader absorption to harvest more of the solar spectrum. Here we find a counter-intuitive narrowing that has not been reported in the literature so far. The case of extinction of a particle in an absorbing medium has been described previously [49–51]; however, the linewidth narrowing observed for the plasmonic resonance of a metal (also absorbing) particle in an absorbing medium has not been described. Past works considered the case where the surrounding medium was weakly absorbing for practical benefit. In this work, we demonstrate that adding a lossy material around a plasmonic particle can actually reduce the linewidth of the plasmonic resonance and increase the scattering peak. We demonstrate this by using numerical simulations of realistic material parameters, as well as analytic analysis.

2. Plasmonic Resonances in Lossy Media

2.1. Rayleigh Scattering

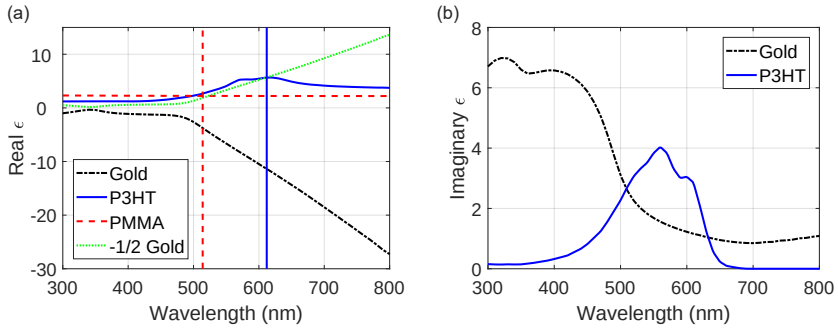

Fig. 1. Relative permittivities for gold, P3HT, and PMMA. (a) The real permittivities. (b) The imaginary permittivities. The vertical solid blue line in (a) corresponds to the plasmon resonance of gold and P3HT at 612 nm determined from the Clausius-Mossotti factor described below. The vertical dashed red line in (a) corresponds to the plasmon resonance of gold and PMMA at 514 nm determined from the Clausius-Mossotti factor. The imaginary part of the permittivity of PMMA is 0.

Figure 1 shows the permittivities of the materials analyzed in this work. P3HT (an organic polymer commonly used in photovoltaics) and gold are both lossy dispersive materials, while PMMA is considered as a non-lossy, non-dispersive material. Figure 2 shows the cross sections of a 10 nm diameter gold nanoparticle embedded in PMMA and 10 nm gold in P3HT predicted by Rayleigh scattering theory.

The theory of scattering by nanoparticles has been established for over a century [52–54]. For particles much smaller than the wavelength of incident light, the quasi-static approximation holds (vanishing time derivatives in Maxwell's equations) and the physics of light scattering is accurately represented with the well known Rayleigh scattering formulas (in SI units) .

$$C_{\text{scat}} = \frac{1}{6\pi}\left(\frac{2\pi}{\lambda}\right)^4 \left|\frac{\alpha}{\epsilon_0}\right|^2 \tag{2}$$

A large scattering cross section means a large portion of incident light is scattered from the nanoparticle. There is a strong dependence on the wavelength of incident light λ as well as the dipole polarizability of the particle α.

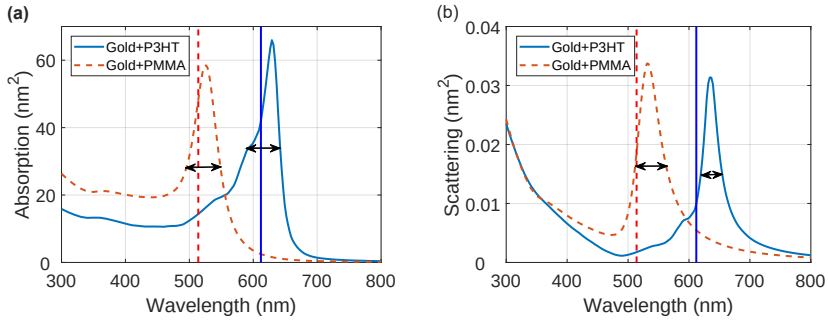

Fig. 2. Cross Sections from Rayleigh scattering formulas, Eqs. 2-5. (a) The absorption cross section of a 10 nm gold sphere embedded in P3HT and 10 nm gold in PMMA. (b) The scattering cross section of a 10 nm gold sphere embedded in P3HT and 10 nm gold in PMMA. For both (a) and (b) the vertical solid blue line represents the gold and P3HT plasmonic resonance and the vertical dashed red line shows the gold and PMMA plasmonic resonance. The black horizontal double arrow lines show the full width at half the maximum of each of the peaks. The gold nanoparticle has a geometric cross section of 7.85×10^{-17} m^2 (πa^2 with $a = 5 \times 10^{-9}$ m).

$$C_{\text{abs}} = \frac{2\pi}{\lambda} \text{Im}\left(\frac{\alpha}{\epsilon_0}\right) \tag{3}$$

Im is the imaginary part of what follows in the brackets. $\epsilon_0 = 8.85 \times 10^{-12}$ is the permittivity of free space.

$$\alpha = 4\pi a^3 \epsilon_{\text{CM}} \epsilon_0 \tag{4}$$

α is the dipole polarizability of the nanoparticle of radius a obtained using the quasi-static approximation. The quasi-static approximation assumes the incident field is constant over the entire nanoparticle at any given time, and so it breaks down for large particle sizes comparable to the wavelength of incident light. Within the dipole polarizability lies the heart of the plasmonics of small nanoparticles, the Clausius-Mossotti factor ϵ_{CM} [55].

$$\epsilon_{\text{CM}} = \frac{\epsilon_1 - \epsilon_2}{\epsilon_1 + 2\epsilon_2} \tag{5}$$

The plasmonic resonance occurs for materials where ϵ_1 (relative permittivity of the nanosphere) and ϵ_2 (relative permittivity of the surrounding medium) maximize this term. The Clausius-Mossotti factor is maximized when the following relation is approximately held:

$$\epsilon_1 = -2\epsilon_2 \tag{6}$$

Rayleigh scattering theory was used to find the absorption and scattering cross sections of 10 nm diameter spherical gold nanoparticles embedded in two different media. The vertical lines in Figure 1(a) show the cases where $\text{Re}(\epsilon_1 + 2\epsilon_2) = 0$, which is the real part satisfying Eq. 6. Figure 1(b) shows the imaginary part of the permittivity corresponding to losses for P3HT and gold. PMMA is not shown because it is assumed to be lossless in this regime.

From Figure 2 we see that the resonances are shifted, as expected from the clausius-Mossotti relation. The resonances are not exactly at the position of the vertical line in Figure 1(a) due to the strong dispersion in the permittivity. As mentioned earlier, the common belief is that adding losses to a plasmonic system will broaden plasmonic resonances. Surprisingly, Rayleigh

scattering theory predicts a linewidth of 50 nm for the scattering cross section of gold in PMMA and 35 nm for the scattering cross section of gold in P3HT (the full width at half maximum was used as a measure for the narrowness of the peaks). Rayleigh theory also predicts plasmonic peaks of nearly the same magnitude for both gold in PMMA and P3HT. In the numerical analysis below, we will see that this gives a large underestimate for the scattering and is a failure of this simple theory for this lossy case.

2.2. *Loss in the Circuit Model*

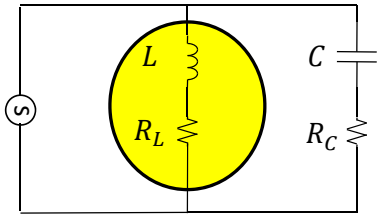

Fig. 3. Equivalent nanocircuit for a metal nanoparticle surrounded by a lossy medium. The resistances in the circuit are associated with the material loss. If neither material is lossy then the resistances are 0.

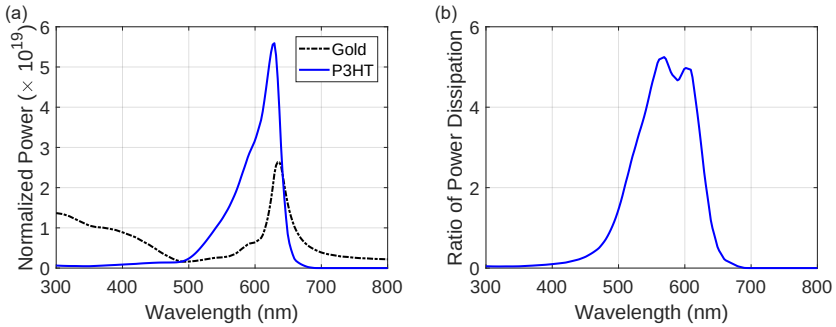

Fig. 4. Optical absorption results of a nanocircuit consisting of a 10 nm gold sphere inductor and surrounding P3HT capacitor. (a) The power absorbed by each circuit element, normalized by the square of the incident field strength $|\mathbf{E}_0|^2$. (b) The ratio of the power absorbed in P3HT to the power absorbed in gold.

Figure 3 shows how a nanoparticle surrounded by an absorbing material can be treated as a nanocircuit [19]. The resistors are placed in series to ensure that each branch represents a different physical material; that is, to avoid shunting. The metal plays the role of an effective inductor (negative capacitor), while the material outside acts as a capacitor in parallel with the inductor. Such a circuit describes a gold nanosphere surrounded by P3HT.

Figure 4 shows how the power dissipation is partitioned between the gold and the P3HT nanocircuit. We see that the circuit model predicts a sharp peak in absorbed power for the gold and P3HT system. We also see that between 550 and 600 nm, the P3HT is absorbing 5 times more power than the gold. This shows the effectiveness of the gold-P3HT combination in photovoltaic applications where it is desirable for the surrounding medium to absorb most of the incident light.

The current, impedance, and potential difference in the circuit are given by [19]:

$$I_L = -j\pi a^2 \omega \epsilon_0 \epsilon_1 \epsilon_{\mathrm{CM}} |\mathbf{E}_0| \tag{7}$$

$$I_C = -j2\pi a^2 \omega \epsilon_0 \epsilon_2 \epsilon_{\mathrm{CM}} |\mathbf{E}_0| \tag{8}$$

$$V = a \epsilon_{\mathrm{CM}} |\mathbf{E}_0| \tag{9}$$

where I_L is the current through the inductor, I_C is the current through the capacitor, V is the potential difference across the circuit, j is the imaginary unit, ω is the incident field frequency, a is the radius of the gold nanoparticle, $|\mathbf{E}_0|$ is the magnitude of the incident electric field and ϵ_1 and ϵ_2 are the relative permittivities of the inductor and capacitor materials. The model assumes linear polarization where the polarization of the field is aligned with the voltage across the capacitor and inductor parts of the circuit.

The power absorbed in each element is given by:

$$P_L = I_L^* V = j\pi a^3 \omega \epsilon_0 \epsilon_1 |\epsilon_{\mathrm{CM}}|^2 |\mathbf{E}_0|^2 \tag{10}$$

$$P_C = I_C^* V = j2\pi a^3 \omega \epsilon_0 \epsilon_2 |\epsilon_{\mathrm{CM}}|^2 |\mathbf{E}_0|^2 \tag{11}$$

Notice that when both of the materials are non-absorbing, then we have purely reactive power in the circuit and there is no power dissipated, as expected in an LC circuit. For materials with loss, there is dissipation.

The relevance of the circuit model was to identify the partitioning of the absorption between the metal and the surrounding material. While the model gives some idea about how this partitioning takes place, it does not predict accurately the results because it is based on the quasi-static model derived for a lossless surrounding medium.

2.3. Numerical Simulations

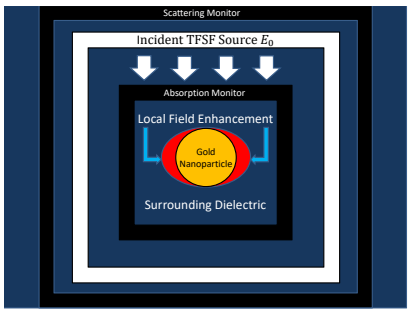

Fig. 5. 2D representation of the layout of the FDTD simulations used for this work.

Figure 5 shows a schematic representation of a finite-difference time-domain (FDTD) simulation for calculating the absorption and losses associated with a gold nanoparticle in a (lossy) dielectric medium. We used a commercial package (Lumerical FDTD version 8.21.1854). The simulation consists of a 10 nm diameter gold nanoparticle surrounded by a dielectric material. There is a box of 2D power monitors of side length 17.5 nm to measure absorbed power, a total field scatter field source (TFSF) with side length 25 nm and another box of 2D power monitors to measure the scattering with a dimension of 250 nm. The TFSF sources light is in the range of 300 to 1000 nm. The TFSF source was injected in the y-axis and polarized in the z-direction.

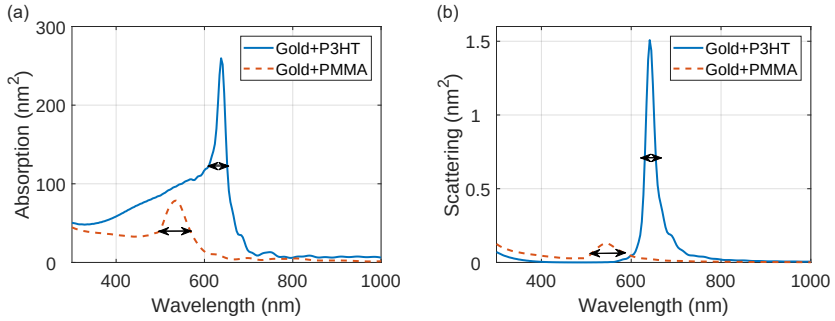

Fig. 6. Cross Sections from FDTD simulations. (a) The absorption cross sections of a single 10 nm gold sphere in P3HT and a single 10 nm gold sphere in PMMA. (b) The scattering cross sections of a single 10 nm gold sphere in P3HT and a single 10 nm gold sphere in PMMA. The black horizontal double arrow lines show the full width at half the maximum of each of the peaks.

The simulation used a time step of 0.002 fs, and a minimum mesh step of 0.25 nm. There was a 0.5 nm mesh used within the TFSF region. The mesh refinement type used was conformal variant 1 for faster convergence on the boundary of the gold nanoparticle. Symmetric boundary conditions were used to significantly reduce simulation time. We used the default 8 layer PML for our FDTD simulation boundaries.

Figure 6 shows the cross section data for each of the simulations that were run in FDTD. Rayleigh scattering theory and FDTD simulations yield similar cross sections for PMMA; however, for the lossy P3HT, they are very different. The absorption cross section peak of gold in PMMA and the absorption cross section peak of gold in P3HT are comparable in magnitude when using Rayleigh scattering theory, but in the FDTD simulations, we see that P3HT has an absorption cross section peak that is 3 times larger than PMMA. Rayleigh scattering theory also predicts scattering cross section peaks for gold in PMMA and gold in P3HT that are similar in magnitude. In the FDTD simulations, the P3HT scattering cross section peak is an order of magnitude larger than the PMMA scattering cross section peak. The large shoulder from 400 to 600 nm in the absorption cross section is accounted for by the absorption of pure P3HT surrounding the gold. This was verified with a simulation where the absorption monitor and TFSF source had their dimensions reduced and there was the expected reduction in the shoulder.

We performed simulations for larger gold particles in P3HT (20 nm) showing similar results. The scattering cross section linewidth was 21 nm and the peak was 4 nm red shifted from that of the 10 nm gold in P3HT. The absorption cross section linewidth was 32 nm and the peak was red shifted by 4 nm from that of 10 nm gold in P3HT.

3. Discussion

Perhaps the most surprising result from the FDTD simulations is the large scattering peak of gold and P3HT. Generally, smaller nanoparticles are known to have insignificant scattering compared to absorption. This is considered in photovoltaics where large nanoparticles are used to scatter light to increase optical path length in the device while smaller nanoparticles are used enhance absorption in the device near the particles [56]. From Eqs. 2-4 we see how the absorption and scattering cross section scale with the nanoparticle radius a.

$$C_{\text{abs}} \propto a^3 \tag{12}$$

$$C_{\text{scat}} \propto a^6 \tag{13}$$

So there is typically an absorbing regime for small a and a scattering regime for large a. For 10 nm gold in P3HT, the scattering cross section is still two orders of magnitude lower than the absorption cross section; however, for a metal-dielectric composite with a large enough scattering peak, there may not be an absorption dominant regime, at least at the peak wavelength.

Next we consider the mechanism of peak narrowing. Looking at Figure 1 it is seen that gold is very dispersive for wavelengths greater than 500 nm, P3HT is dispersive from 300 to 650 nm and PMMA is non-dispersive. It is the strong dispersion in both P3HT and gold that leads rapid variations in the Clausius-Mossotti factor and narrower peaks.

The numerator of Eq. 5 is often ignored, but for seeking small resonance linewidths this term becomes important. For the ideal physical cross section peak, the dispersion of each of the materials would be such that moving off resonance would result in changing the Clausius-Mossotti from maximum directly to a minimum. Minima in both scattering and absorption cross sections exist when the Clausius-Mossotti factor is 0. So, if for some combination of nanoparticle and surrounding medium $\epsilon_1(\lambda_1) \approx \epsilon_2(\lambda_1)$ then the permitivitties move towards $\epsilon_1(\lambda_2) \approx -2\epsilon_2(\lambda_2)$ and then again the permitivitties move back to $\epsilon_1(\lambda_3) \approx \epsilon_2(\lambda_3)$ in a short wavelength span $\Delta\lambda = \lambda_3 - \lambda_1$, there will be a very narrow cross section, regardless of the loss of the surrounding medium. The more dispersive a material, the quicker the material permittivities are changing with wavelength and the faster the composite can move through plasmonic resonance. This highlights the importance of dispersion in creating narrow resonances.

4. Conclusion

Here we have shown that a surrounding lossy medium can narrow the plasmonic resonances, as well as increase their amplitude dramatically. This was shown clearly with FDTD simulations, and some of the features are represented by quasi-static theory; however, the latter is clearly not suitable for obtaining accurate results and greatly underestimates the narrowing and enhanced scattering. We note that the comprehensive simulations agree well with the quasistatic response when there is no loss in the surrounding material, but the results are very different for the lossy case. Since the convergence of the FDTD was confirmed, the approach accurately represents MaxwellâĂŹs equations and therefore the quasistatic approach fails for this regime. While we use P3HT as a model system, other absorbing materials may prove to show this effect more vividly. Nanomaterials with abnormally narrow cross sections can see applications in bioimaging/biosensing, where they allow for a higher degree of multiplexing, and also in photovoltaics for greatly enhanced absorption and scattering (both can be utilized) at a desired section of the optical spectrum. Further theoretical development is required to analytically understand the case where both the metal and dielectric materials are lossy and quasi-normal mode theory is a promising way forward [57, 58].

Funding

This work is supported by the NSERC (Canada) CREATE Materials for Enhanced Energy Technologies (MEET) program and the NSERC Discovery Grants program.

Disclosures

The authors declare that there are no conflicts of interest related to this article.

References

1. W. Hu, E. Liang, P. Ding, G. Cai, and Q. Xue, "Surface plasmon resonance and field enhancement in #-shaped gold wires metamaterial," Opt. Express **17**, 21843–21849 (2009).

2. K. Kneipp, Y. Wang, H. Kneipp, L. T. Perelman, I. Itzkan, R. R. Dasari, and M. S. Feld, "Single molecule detection using surface-enhanced raman scattering (sers)," Phys. Rev. Lett. **78**, 1667–1670 (1997).
3. S. Nie and S. R. Emory, "Probing single molecules and single nanoparticles by surface-enhanced raman scattering," science **275**, 1102–1106 (1997).
4. X. Zhang, W. J. Salcedo, M. M. Rahman, and A. G. Brolo, "Surface-enhanced raman scattering from bowtie nanoaperture arrays," Surf. Sci. **676**, 39–45 (2018).
5. M. L. Juan, M. Righini, and R. Quidant, "Plasmon nano-optical tweezers," Nat. Photonics **5**, 349 (2011).
6. Y. Pang and R. Gordon, "Optical trapping of a single protein," Nano letters **12**, 402–406 (2011).
7. B. J. Roxworthy, K. D. Ko, A. Kumar, K. H. Fung, E. K. Chow, G. L. Liu, N. X. Fang, and K. C. Toussaint Jr, "Application of plasmonic bowtie nanoantenna arrays for optical trapping, stacking, and sorting," Nano Lett. **12**, 796–801 (2012).
8. Y. Tang, X. Zeng, and J. Liang, "Surface plasmon resonance: an introduction to a surface spectroscopy technique," J. Chem. Educ. **87**, 742–746 (2010).
9. A. Ahmed and R. Gordon, "Single molecule directivity enhanced raman scattering using nanoantennas," Nano Lett. **12**, 2625–2630 (2012).
10. A. G. Brolo, "Plasmonics for future biosensors," Nat. Photonics **6**, 709 (2012).
11. W. Cai, T. Gao, H. Hong, and J. Sun, "Applications of gold nanoparticles in cancer nanotechnology," Nanotechnology, Sci. Appl. **1**, 17 (2008).
12. M. D. Arnold and R. J. Blaikie, "Subwavelength optical imaging of evanescent fields using reflections from plasmonic slabs," Opt. Express **15**, 11542–11552 (2007).
13. J. W. Nelson, G. R. Knefelkamp, A. G. Brolo, and N. C. Lindquist, "Digital plasmonic holography," Light. Sci. & Appl. **7**, 52 (2018).
14. C. Wang, P. Gao, Z. Zhao, N. Yao, Y. Wang, L. Liu, K. Liu, and X. Luo, "Deep sub-wavelength imaging lithography by a reflective plasmonic slab," Opt. Express **21**, 20683–20691 (2013).
15. N. Engheta, A. Alù, and A. Salandrino, "Nanocircuit elements, nano-transmission lines and nano-antennas using plasmonic materials in the optical domain," in *IWAT 2005. IEEE International Workshop on Antenna Technology: Small Antennas and Novel Metamaterials, 2005,* (IEEE, 2005), pp. 165–168.
16. S. A. Maier and H. A. Atwater, "Plasmonics: localization and guiding of electromagnetic energy in metal/dielectric structures," J. Appl. Phys. **98**, 10 (2005).
17. E. Ozbay, "Plasmonics: merging photonics and electronics at nanoscale dimensions," Science **311**, 189–193 (2006).
18. N. Engheta, "Circuits with light at nanoscales: optical nanocircuits inspired by metamaterials," Science **317**, 1698–1702 (2007).
19. N. Engheta, A. Salandrino, and A. Alù, "Circuit elements at optical frequencies: nanoinductors, nanocapacitors, and nanoresistors," Phys. Rev. Lett. **95**, 095504 (2005).
20. B. P. Rand, P. Peumans, and S. R. Forrest, "Long-range absorption enhancement in organic tandem thin-film solar cells containing silver nanoclusters," J. Appl. Phys. **96**, 7519–7526 (2004).
21. V. E. Ferry, J. N. Munday, and H. A. Atwater, "Design considerations for plasmonic photovoltaics," Adv. Mater. **22**, 4794–4808 (2010).
22. M. R. Jones, K. D. Osberg, R. J. Macfarlane, M. R. Langille, and C. A. Mirkin, "Templated techniques for the synthesis and assembly of plasmonic nanostructures," Chem. Rev. **111**, 3736–3827 (2011).
23. M. Notarianni, K. Vernon, A. Chou, M. Aljada, J. Liu, and N. Motta, "Plasmonic effect of gold nanoparticles in organic solar cells," Sol. Energy **106**, 23–37 (2014).
24. J. Becker, I. Zins, A. Jakab, Y. Khalavka, O. Schubert, and C. Sönnichsen, "Plasmonic focusing reduces ensemble linewidth of silver-coated gold nanorods," Nano letters **8**, 1719–1723 (2008).
25. Y. Chu, E. Schonbrun, T. Yang, and K. B. Crozier, "Experimental observation of narrow surface plasmon resonances in gold nanoparticle arrays," Appl. Phys. Lett. **93**, 181108 (2008).
26. Y. Gao, Z. Xin, Q. Gan, X. Cheng, and F. J. Bartoli, "Plasmonic interferometers for label-free multiplexed sensing," Opt. express **21**, 5859–5871 (2013).
27. J. B. Khurgin, "How to deal with the loss in plasmonics and metamaterials," Nat. Nanotechnol. **10**, 2 (2015).
28. P. R. West, S. Ishii, G. V. Naik, N. K. Emani, V. M. Shalaev, and A. Boltasseva, "Searching for better plasmonic materials," Laser & Photonics Rev. **4**, 795–808 (2010).
29. S. A. Maier, *Plasmonics: fundamentals and applications* (Springer Science & Business Media, 2007).
30. S. Link and M. A. El-Sayed, "Size and temperature dependence of the plasmon absorption of colloidal gold nanoparticles," The J. Phys. Chem. B **103**, 4212–4217 (1999).
31. M. Aeschlimann, "Electron dynamics in metallic nanoparticles," Encycl. Nanosci. Nanotechnol. **3**, 29–40 (2004).
32. R. C. Monreal, S. P. Apell, and T. J. Antosiewicz, "Surface scattering contribution to the plasmon width in embedded ag nanospheres," Opt. express **22**, 24994–25004 (2014).
33. M. G. Blaber, M. D. Arnold, and M. J. Ford, "Search for the ideal plasmonic nanoshell: the effects of surface scattering and alternatives to gold and silver," The J. Phys. Chem. C **113**, 3041–3045 (2009).
34. H. Hövel, S. Fritz, A. Hilger, U. Kreibig, and M. Vollmer, "Width of cluster plasmon resonances: bulk dielectric functions and chemical interface damping," Phys. Rev. B **48**, 18178 (1993).
35. C. Hendrich, J. Bosbach, F. Stietz, F. Hubenthal, T. Vartanyan, and F. Träger, "Chemical interface damping of surface plasmon excitation in metal nanoparticles: a study by persistent spectral hole burning," Appl. Phys. B **76**, 869–875

(2003).
36. B. Foerster, A. Joplin, K. Kaefer, S. Celiksoy, S. Link, and C. SoÌĹnnichsen, "Chemical interface damping depends on electrons reaching the surface," ACS Nano **11**, 2886–2893 (2017).
37. T. Klar, M. Perner, S. Grosse, G. Von Plessen, W. Spirkl, and J. Feldmann, "Surface-plasmon resonances in single metallic nanoparticles," Phys. Rev. Lett. **80**, 4249 (1998).
38. J. A. Scholl, A. L. Koh, and J. A. Dionne, "Quantum plasmon resonances of individual metallic nanoparticles," Nature **483**, 421 (2012).
39. U. Kreibig and L. Genzel, "Optical absorption of small metallic particles," Surf. Sci. **156**, 678–700 (1985).
40. M. M. Alvarez, J. T. Khoury, T. G. Schaaff, M. N. Shafigullin, I. Vezmar, and R. L. Whetten, "Optical absorption spectra of nanocrystal gold molecules," The J. Phys. Chem. B **101**, 3706–3712 (1997).
41. M. Noginov, G. Zhu, M. Bahoura, J. Adegoke, C. Small, B. Ritzo, V. Drachev, and V. Shalaev, "Enhancement of surface plasmons in an ag aggregate by optical gain in a dielectric medium," Opt. Lett. **31**, 3022–3024 (2006).
42. K. Sathiyamoorthy, K. Sreekanth, R. Sidharthan, V. Murukeshan, and B. Xing, "Surface plasmon enhancement in gold nanoparticles in the presence of an optical gain medium: an analysis," J. Phys. D: Appl. Phys. **44**, 425102 (2011).
43. D. J. Bergman and M. I. Stockman, "Surface plasmon amplification by stimulated emission of radiation: quantum generation of coherent surface plasmons in nanosystems," Phys. Rev. Lett. **90**, 027402 (2003).
44. N. I. Zheludev, S. Prosvirnin, N. Papasimakis, and V. Fedotov, "Lasing spaser," Nat. Photonics **2**, 351 (2008).
45. E. I. Galanzha, R. Weingold, D. A. Nedosekin, M. Sarimollaoglu, J. Nolan, W. Harrington, A. S. Kuchyanov, R. G. Parkhomenko, F. Watanabe, Z. Nima, A. S. Biris, A. I. Plekhanov, M. I. Stockman, and V. P. Zharov, "Spaser as a biological probe," Nat. Commun. **8**, 15528 (2017).
46. V. Kochergin, L. Neely, C.-Y. Jao, and H. D. Robinson, "Aluminum plasmonic nanostructures for improved absorption in organic photovoltaic devices," Appl. Phys. Lett. **98**, 73 (2011).
47. M. Stavytska-Barba, M. Salvador, A. Kulkarni, D. S. Ginger, and A. M. Kelley, "Plasmonic enhancement of raman scattering from the organic solar cell material p3ht/pcbm by triangular silver nanoprisms," The J. Phys. Chem. C **115**, 20788–20794 (2011).
48. A. P. Kulkarni, K. M. Noone, K. Munechika, S. R. Guyer, and D. S. Ginger, "Plasmon-enhanced charge carrier generation in organic photovoltaic films using silver nanoprisms," Nano Lett. **10**, 1501–1505 (2010).
49. C. F. Bohren and D. P. Gilra, "Extinction by a spherical particle in an absorbing medium," J. Colloid Interface Sci. **72**, 215–221 (1979).
50. G. Videen and W. Sun, "Yet another look at light scattering from particles in absorbing media," Appl. Opt. **42**, 6724–6727 (2003).
51. M. I. Mishchenko, "Electromagnetic scattering by a fixed finite object embedded in an absorbing medium," Opt. Express **15**, 13188–13202 (2007).
52. Lord Rayleigh, *On the scattering of light by small particles* (1871).
53. G. Mie, "Die optischen eigenschaften kolloider goldlösungen," Colloid & Polym. Sci. **2**, 129–133 (1907).
54. G. Mie, "Beiträge zur optik trüber medien, speziell kolloidaler metallösungen," Annalen der Physik **330**, 377–445 (1908).
55. T. Honegger, K. Berton, E. Picard, and D. Peyrade, "Determination of clausius–mossotti factors and surface capacitances for colloidal particles," Appl. Phys. Lett. **98**, 181906 (2011).
56. K. R. Catchpole, , and A. Polman, "Plasmonic solar cells," Opt. Express **16**, 21793–21800 (2008).
57. C. Sauvan, J.-P. Hugonin, I. S. Maksymov, and P. Lalanne, "Theory of the spontaneous optical emission of nanosize photonic and plasmon resonators," Phys. Rev. Lett. **110**, 237401 (2013).
58. R.-C. Ge, P. T. Kristensen, J. F. Young, and S. Hughes, "Quasinormal mode approach to modelling light-emission and propagation in nanoplasmonics," New J. Phys. **16**, 113048 (2014).